ACS OMEGA

Open Access

http://pubs.acs.org/journal/acsodf

Article

Corosolic Acid Induced Apoptosis via Upregulation of Bax/Bcl-2 Ratio and Caspase-3 Activation in Cholangiocarcinoma Cells

Onanong Jedram, Pornpattra Maphanao, Kun Karnchanapandh, Panupong Mahalapbutr, Raynoo Thanan, and Chadamas Sakonsinsiri*

Cite This: *ACS Omega* 2024, 9, 1278−1286

Read Online

ACCESS | Metrics & More | Article Recommendations

ABSTRACT: Cholangiocarcinoma (CCA), an aggressive malignancy arising from the biliary epithelium, exhibits a high incidence in Thailand. CCA usually lacks specific symptoms and is typically diagnosed in its advanced stages, presenting significant treatment challenges. Current CCA therapeutic options, including surgery, chemotherapy, and radiation, have limited success rates and often cause side effects. Nature-derived compounds hold promise for reducing undesirable adverse effects and are an excellent source of anticancer drugs. Corosolic acid (CA), a triterpenoid found in *Lagerstroemia speciosa* L. leaves, exhibits anticancer properties; however, the effectiveness of CA against CCA and its molecular mechanisms remained unexplored. Herein, the anti-CCA and apoptosis-inducing effects of CA were investigated using various techniques, *i.e.*, the MTT assay, flow cytometry with FITC-labeled Annexin V (Annexin V-FITC) and propidium iodide double staining, JC-1 staining, western blot analysis, caspase-3 activity assay, and molecular dynamics (MD) simulations. CA inhibited the proliferation of KKU-213A and KKU-213B CCA cells and triggered apoptosis through alterations in mitochondrial membrane potential (ΔΨm), and increases in the Bax/Bcl-2 expression ratio, cytochrome *c* release, and caspase-3 activity. As indicated by MD simulations, CA has the potential to bind to Bcl-2 through hydrogen bonds between amino acid residues R146 and N143. These findings underscore the potential of CA as a promising candidate for treatment of CCA.

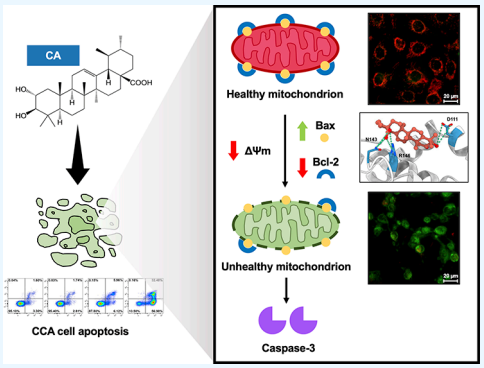

INTRODUCTION

Cholangiocarcinoma (CCA), a malignancy originating from the epithelial lining of the biliary tract, is rare on a global scale; however, it exhibits the highest incidence in South East Asian countries, notably Thailand.[1] Infection with *Opisthorchis viverrini* is identified as an important risk factor for CCA in Thailand.[2] Surgical resection is the most curative treatment option for CCA, although patients in advanced stages are often ineligible for surgical therapies.[3] The combination of gemcitabine plus cisplatin (GC) is currently used as a standard regimen for unresectable CCA and has satisfactory overall response rates. However, when compared to gemcitabine alone, the GC regimen only added a few months to disease-free survival.[4] It can result in adverse effects such as neutropenia, fatigue, and thrombocytopenia.[5] As a result, there is a concerted effort within the field to discover new and effective drugs for the treatment of CCA. Employing a naturally produced plant-derived compound with anticancer properties can provide an alternative therapeutic approach with fewer adverse effects.

Cancer can resist apoptosis, resulting in uncontrolled proliferation and tumor formation, highlighting the need to understand its mechanisms to develop new cancer therapeutics.[6] Multiple morphological changes are evident during apoptosis, such as cell shrinkage, decreased cell volume, chromatin condensation, vesicle formation, and apoptotic bodies (ABs) formation.[7] Phosphatidylserine translocation to the outer surface of the plasma membrane has been seen as a distinctive characteristic of apoptotic cells.[8] In addition, mitochondria play a crucial role in the mechanism of apoptotic cell death, which typically involves the pro- and antiapoptotic proteins. Changes in the levels of Bcl-2 and Bax, two prominent members within the Bcl family, can collapse the mitochondrial membrane potential (ΔΨm) and the subsequent release of cytochrome *c*, inducing apoptosis.[9] Increasing the Bax/Bcl-2 ratio significantly activates apoptotic signaling pathway.[10,11] The release of cytochrome *c* from mitochondria is a crucial mechanism for activating caspases, cysteine proteases cleaving proteins after aspartate residues. In the

Received: September 29, 2023
Revised: November 9, 2023
Accepted: November 30, 2023
Published: December 19, 2023

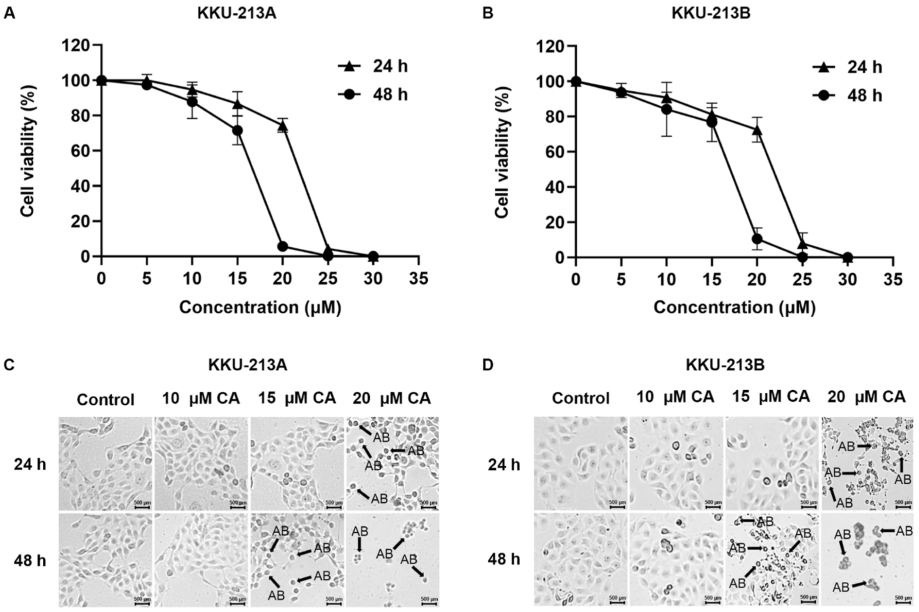

Figure 1. Effect of CA on cell proliferation in CCA cell lines. KKU-213A (A) and KKU-213B (B) cells were treated with 5−30 μM CA for 24 and 48 h and subsequently subjected to the MTT assay. Morphological changes in KKU-213A (C) and KKU-213B cells (D) were visually examined using an inverted microscope. Arrows indicate representative ABs. The images were captured at a magnification of ×50. The presented data represents the mean ± standard deviation from three independent experiments.

cytoplasm, cytochrome *c* combines with caspase-9 and Apaf-1 to form the apoptosome, initiating caspase-9 activation, which, in turn, triggers caspase-3 for apoptosis execution.[12]

Corosolic acid (CA) is a pentacyclic triterpenoid found predominantly in the leaves of *Lagerstroemia speciosa* L., commonly known as banaba.[13] Accumulating evidence suggests that CA has anticancer effects through interfering with several processes, such as cell proliferation, angiogenesis, invasion, metastasis, and apoptosis.[14−18] CA induced apoptosis in gastric cancer by inhibiting the NF-κB pathway[19] and in colorectal cancer by activating mitochondria-mediated and caspase-dependent pathways with decreased expression levels of p65, Fas, caspase -8, -9, and -3, and Bcl-2 and increased expression of Bax.[20] In addition, CA triggered apoptosis by elevating reactive oxygen species (ROS) levels, lowering Bcl-2 levels in lung cancer,[21] and activating caspase-3/7, -8, and -9 in osteosarcoma.[22]

This study sought to investigate the anticancer activities of CA and elucidate its underlying molecular mechanism in CCA. In KKU-213A and KKU-213B cell lines, the cytotoxic effect of CA was evaluated using the 3-(4,5-dimethyl-2-thiazolyl)-2,5-diphenyl-2H-tetrazolium bromide (MTT) assay. Flow cytometry using Annexin V-FITC/propidium iodide (PI) staining was used to detect phosphatidylserine externalization on apoptotic cells. Changes in $\Delta\Psi$m were assessed using 5,5′,6,6′-tetrachloro-1,1′,3,3′-tetraethylbenzimidazolylcarbocyanine iodide (JC-1) stanning and confocal microscopy. Using western blotting, the apoptosis-related proteins Bax, Bcl-2, and cytochrome *c* were examined, while the caspase-3 activity was measured using a caspase-3 activity assay kit. Molecular dynamics (MD) simulations were employed to determine the probable molecular targets and binding interactions of CA and Bcl-2.

RESULTS AND DISCUSSION

Evaluation of the Cytotoxic Effect of CA. KKU-213A and KKU-213B cells were exposed to various concentrations of CA ranging from 0 to 30 μM for 24 and 48 h, and their cytotoxicity was determined using the MTT assay. The results showed that CA inhibited CCA proliferation in a dose- and time-dependent manner (Figure 1A,B). At 24 and 48 h, the IC_{50} values for KKU-213A cells were 21.45 ± 0.35 and 16.40 ± 0.53 μM, respectively. Similarly, the IC_{50} values of KKU-213B cells for 24 and 48 h were 21.40 ± 0.92 and 17.54 ± 0.73 μM, respectively. In addition, when exposed to 20 μM CA for 24 h and 15 μM for 48 h, both cell lines exhibited morphological changes, including cell shrinkage and the formation of AB, as observed using an inverted microscope (Figure 1C,D). CA exhibited comparable IC_{50} values (approximately 20−40 μM) to those determined in osteosarcoma,[22] glioblastoma,[23] hepatocellular carcinoma,[15] liver cancer,[16,24] breast cancer,[25] and prostate cancer.[26]

Detection of Apoptotic Cells Induced by CA. The observed morphological changes open up avenues for further investigation into the mechanisms and pathways involved in CA-induced apoptosis in CCA cells. Flow cytometric analysis using Annexin V-FITC/PI double staining was performed. Annexin V-FITC binds to phosphatidylserine in apoptotic cells, while PI specifically labels nucleic acids when the plasma membranes of necrotic cells rupture. The resulting staining patterns were classified into four categories: viable cells (Annexin V-FITC-/PI-), early apoptotic cells (Annexin V-FITC+/PI-), late apoptotic cells (Annexin V-FITC+/PI+), and necrotic cells (Annexin V-FITC-/PI+). It was found that when KKU-213A cells were exposed to CA at concentrations of 15, 20, and 25 μM, the early and late apoptotic cell percentages were 4.90, 4.55, 12.08, and 89.30%, respectively (Figure 2). In the case of the KKU-213B cell line, treatment with 15, 20, and 25 μM CA resulted in the total percentages of apoptotic cells as 3.48, 3.45, 16.08, and, 74.65%, respectively. CA induced apoptosis in both KKU-213A and KKU-213B cell lines in a dose-dependent manner, as evidenced by increased percentages of early and late apoptotic cells. At a concentration of 25 μM CA, there was a notable and significant increase in

https://doi.org/10.1021/acsomega.3c07556
ACS Omega 2024, 9, 1278−1286

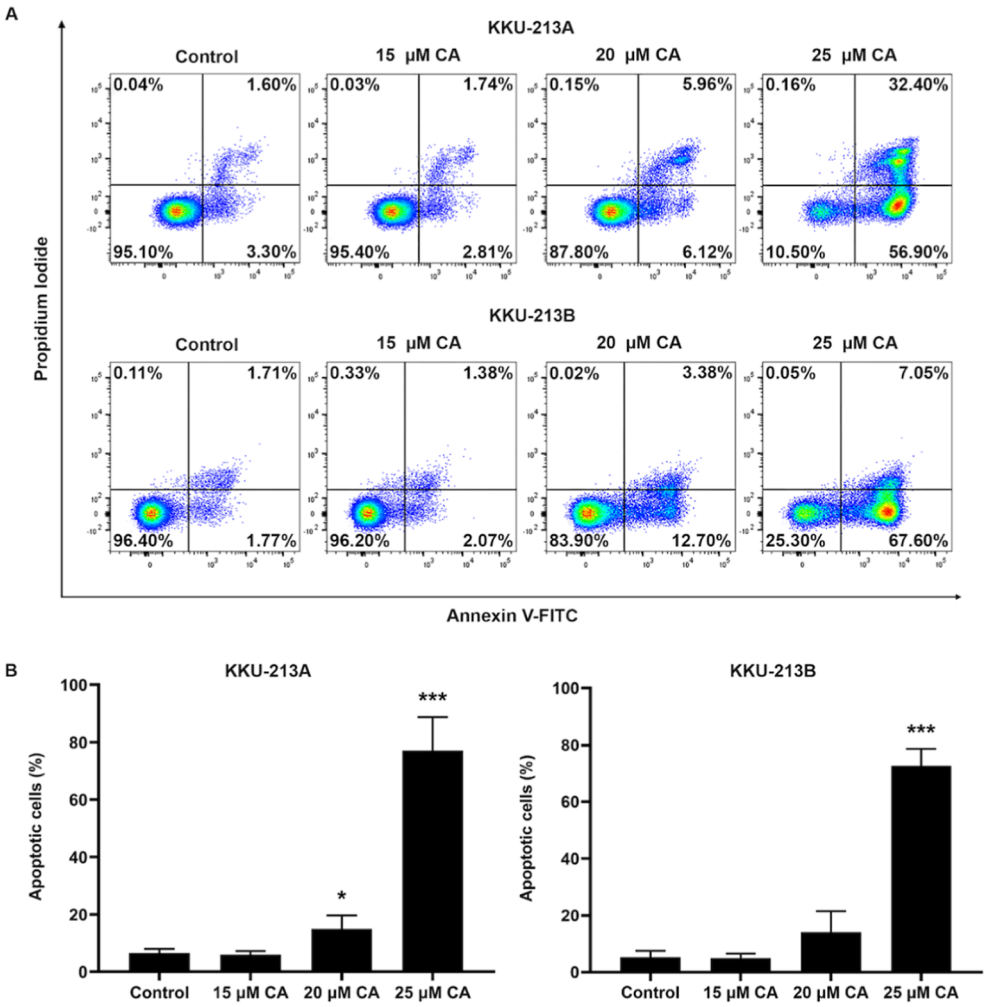

Figure 2. Flow cytometric analysis of apoptosis in CCA cells. (A) Representative data from three independent experiments are shown. KKU-213A and KKU-213B cells were treated with CA at concentrations of 15, 20, and 25 μM for 24 h. Cells were stained with FITC-Annexin V/PI and subjected to flow cytometry. The lower left quadrant shows normal cells, the lower right quadrant shows the early apoptotic cells, the upper right quadrant shows late apoptotic cells, and the upper left quadrant shows necrotic cells. (B) Total apoptotic cell rate was calculated as the rate of both early and late apoptotic cells in KKU-213A and KKU-213B cell lines. Data are presented at the mean ± SD of three independent experiments, $^{*}P < 0.05$ and $^{***}P < 0.001$ versus control.

apoptotic cells in both of the tested cell lines when compared to the control group. These results supported the morphological changes, especially the presence of ABs observed through an inverted microscope, thereby validating the apoptosis-inducing impact of CA on KKU-213A and KKU-213B cell lines.

Investigation of the Effect of CA on Mitochondrial Membrane Potential Change. The effect of CA on the change in the ΔΨm was evaluated using JC-1 staining and confocal laser scanning microscopy. In healthy cells with a high ΔΨm, JC-1 assumes an aggregated state, resulting in red fluorescence. Conversely, in apoptotic cells, they undergo a transition to a monomeric form, emitting green fluorescence. CA induced a reduction in ΔΨm, as indicated by the shift from red to green fluorescence in CCA cells (Figure 3). When KKU-213A cells were exposed to increasing CA concentrations (15, 20, and 25 μM), a dose-dependent decrease in the red/green fluorescence ratio was observed, indicating a gradual decline in ΔΨm compared to control-untreated cells (Figure 3A). Exposing KKU-213A cells to CA at both 20 and 25 μM resulted in a significant increase in the red/green ratio. KKU-213B cells exhibited a similar trend, where increasing CA concentrations led to a dose-dependent elevation in the red/green fluorescence ratio, indicating a progressive loss of membrane potential (Figure 3B). These findings suggest that CA caused ΔΨm changes in both KKU-213A and KKU-213B CCA cells.

Investigation of the Effect of CA on Bax, Bcl-2, and Cytochrome *c* Levels. The effect of proteins implicated in CA-induced apoptosis on CCA KKU-213A and KKU-213B cells was evaluated using western blotting. Cells were exposed to 20 μM CA for various durations (6, 12, and 24 h). In a time-dependent manner, both KKU-213A and KKU-213B cells treated with CA exhibited an increase in the Bax/Bcl-2 ratio, a pivotal indicator of the initiation of apoptotic processes (Figure 4A,B). Additionally, CA enhanced the release of cytochrome *c* in both CCA cell lines (Figure 4C,D). Consistent with previous studies, our results indicated that elevated Bax/Bcl-2 ratio and increased cytochrome *c* levels are associated with apoptosis.[27−30] CA-induced increases in the Bax/Bcl-2 ratio and cytochrome *c* levels in CCA cells provide

https://doi.org/10.1021/acsomega.3c07556
ACS Omega 2024, 9, 1278−1286

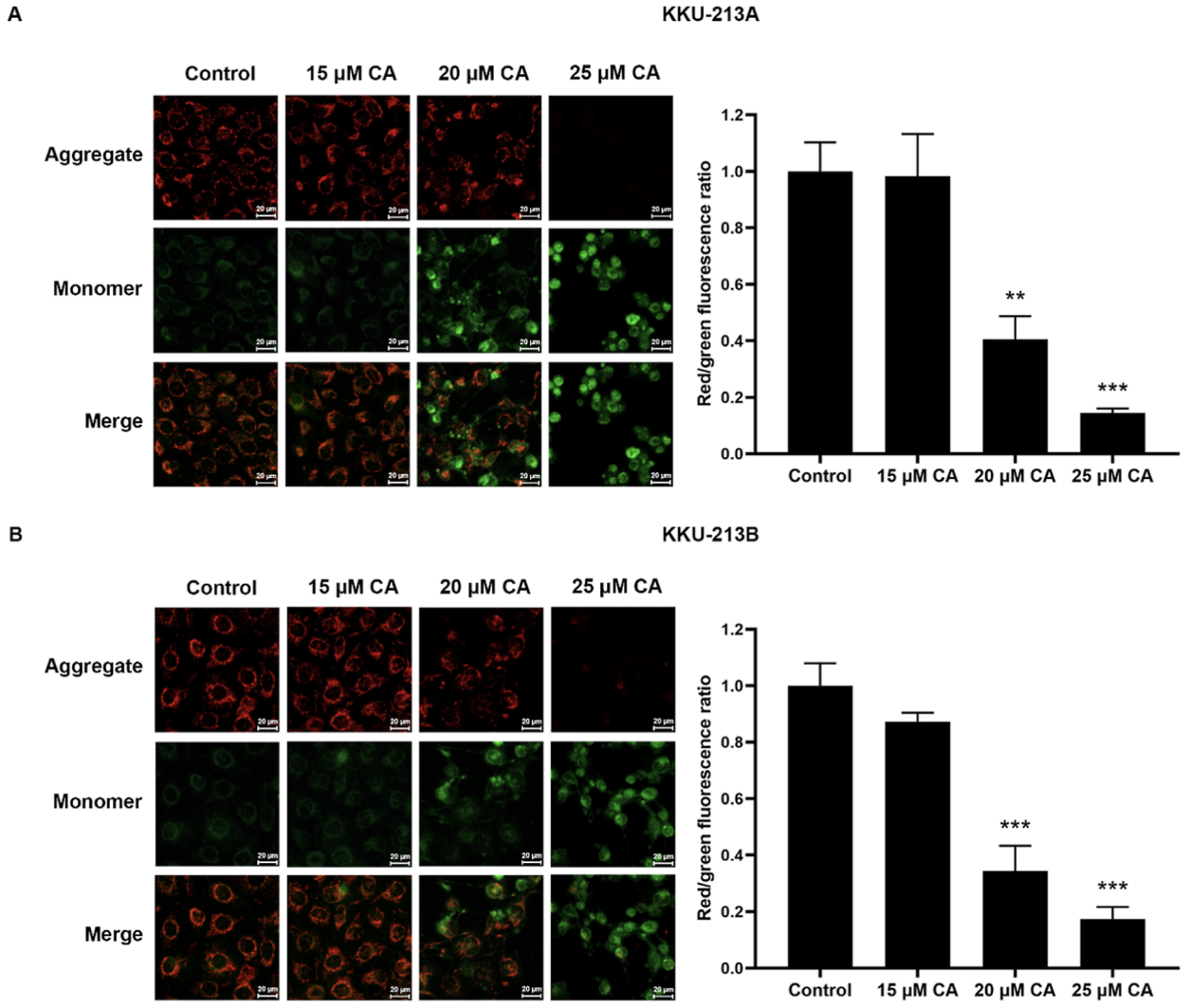

Figure 3. Assessment of $\Delta\Psi$m using JC-1 staining in KKU-213A (A) and KKU-213B (B) cells. Representative images of JC-1 staining are shown, magnification, ×200. Cells were exposed to 15, 20, and 25 μM CA for 24 h and stained with JC-1, a membrane potential sensitive fluorescent dye. Red channel: JC-1 aggregate form; green channel: JC-1 monomeric form; merged images. Red to green fluorescence intensity was quantified using ImageJ software (n = 3 for each group). Data are expressed as mean ± SD of triplicate experiments, ** and *** represent $P < 0.01$ and $P < 0.001$, respectively.

compelling evidence that CA has the capacity to trigger apoptosis through the mitochondria-mediated pathway.

Assessment of the Caspases-3 Activity. As caspase-3 activation is well established as a critical mediator of apoptosis, CCA cells were treated with 20 μM CA for 6, 12, and 24 h, and caspase-3 activity was assessed. CA significantly increased caspase-3 activity in both KKU-213A and KKU-213B cells relative to the control group at 0 h in a time-dependent manner (Figure 5). Therefore, CA induced apoptosis in CCA cells through mitochondria-mediated apoptotic and caspase-dependent pathways.

Evaluation of Stability and Binding Hotspot of the CA/Bcl-2 Complex. The structural stability and dynamic behavior of the CA/Bcl-2 complex were determined using various parameters, including root-mean-square displacement (RMSD), the number of atomic contacts (#contacts) between CA and Bcl-2, and the solvent-accessible surface area (SASA) within 5 Å of ligand. The results showed that the fluctuation of RMSD values, #contacts, and SASA values were relatively low with values of approximately 1.5−2 Å, 10−15, and 400 Å^2, respectively, after 20 ns until the end of the simulation period (Figure 6A), suggesting the high stability of CA/Bcl-2 complex in an aqueous environment. Based on these results, the last 20 ns MD snapshots were extracted for further analyses.

To evaluate the key binding residues involved in the binding of CA to the Bcl-2 target, the per-residue decomposition free energy ($\Delta G_{bind}^{residue}$) was calculated using molecular mechanics/generalized Born surface area (MM/GBSA) method. As shown in Figure 6B, four residues (*i.e.*, F104, Y108, N143, and R146) were associated with the binding interactions of CA. As previously reported, Bcl-2 consists of four different domains: BH1 (residues 136−155), BH2 (residues 187−202), BH3 (residues 97−112), and BH4 (residues 11−30) domains.[31] Consequently, N143 and R146 are located within the BH1 domain of Bcl-2, whereas F104 and Y108 reside in the BH3 domain. Among these four residues, the positively charged R146 exhibited the highest electrostatic contribution to the binding of CA. It should be noted that CA formed strong H-bonds with N143 and R146 amino acid residues of Bcl-2 (more than 80% H-bond occupations, Figure 6C). The residues N143 and R146 of the BH1 domain and F104 and Y108 of the BH3 domain were reported to be critical for

https://doi.org/10.1021/acsomega.3c07556
ACS Omega 2024, 9, 1278−1286

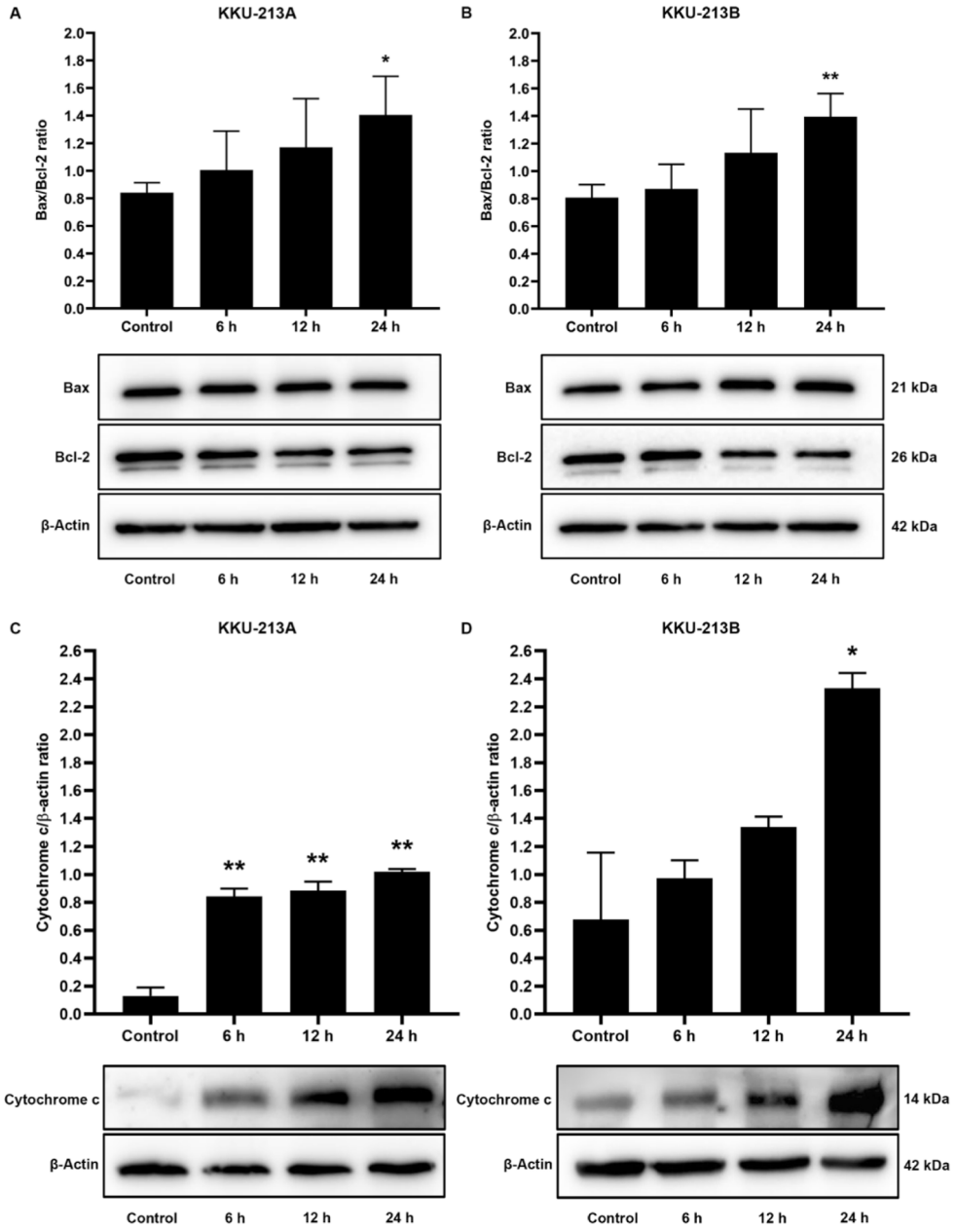

Figure 4. Effects of CA on the Bax/Bcl-2 ratio (A,B) and cytochrome *c* levels (C,D) in KKU-213A and KKU-213B cells after treatment with 20 μM CA for 0−24 h detected using western blot analysis. Data are expressed as mean ± SD of triplicate experiments, * and ** represent $P < 0.05$ and $P < 0.01$, respectively. Representative images of three independent western blot experiments are shown.

binding with (i) small-molecule Bcl-2 inhibitors, including TW-37,[32] 2,3-dicyanophenanone derivatives,[33] disarib,[34] and pyrogallol derivatives;[35] (ii) p53 tumor suppressor protein; and (iii) proapoptotic Bax protein.[36] All of the aforementioned compounds depend on the interaction of amino acid residues located within the BH1 and BH3 domains of Bcl-2. Taken together, these findings suggested the potential for CA to affect Bcl-2, causing apoptosis in CCA cells. However, it is crucial to note the limitations of this work, most notably, the lack of information regarding the binding activity between CA and Bcl-2.

CONCLUSIONS

Our findings unveil, for the first time, the anticancer activity of CA in CCA cells. Specifically, CA inhibited cell proliferation and induced apoptosis primarily through the mitochondria-mediated apoptosis pathway. Moreover, we elucidate the molecular mechanism through which CA influences mitochondria-mediated cell death, involving an increase in the proapoptotic protein Bax-to-antiapoptotic protein Bcl-2 ratio, enhanced cytochrome *c* release, and a decrease in $\Delta\Psi m$, and subsequent activation of caspase-3. MD simulations suggested a potential interaction between CA and Bcl-2. By shedding light on these delicate cellular processes, our study provides a deeper understanding of the underlying antitumor mechanism inherent to CA. Overall, this not only establishes a foundation for potential therapeutic applications of CA in CCA treatment but also holds the promise of paving the way for future developments in CA-based therapeutics.

https://doi.org/10.1021/acsomega.3c07556
ACS Omega 2024, 9, 1278−1286

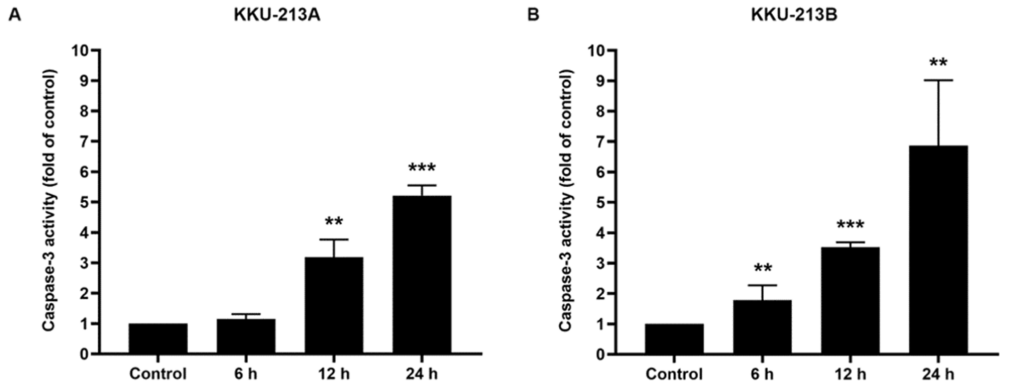

Figure 5. Caspase-3 activity of CA-treated KKU-213A (A) and KKU-213B (B) CCA for 0−24 h. Data are expressed as mean ± SD of triplicate experiments, * and ** represent $P < 0.05$ and $P < 0.01$, respectively.

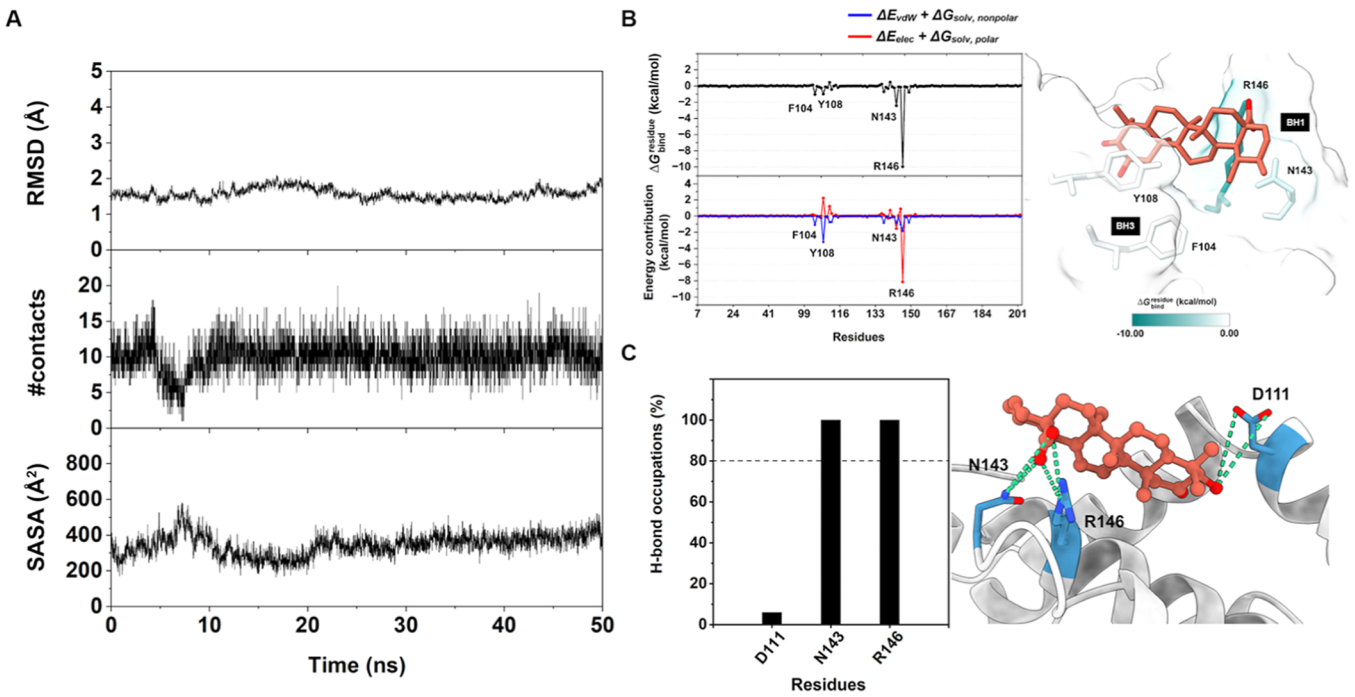

Figure 6. (A) Time evolution of RMSD, #contacts, and SASA of the CA/Bcl-2 complex. (B) (top) $\Delta G_{bind}^{residue}$ of CA in complex with Bcl-2 and (bottom) the vdW ($\Delta E_{vdW} + \Delta G_{solv,nonpolar}$, blue) and electrostatic ($\Delta E_{elec} + \Delta G_{solv,polar}$, red) energy contributions from each residue of Bcl-2 to the binding of CA. (C) Percentage of H-bond occupation of Bcl-2 contributing to the binding of CA.

MATERIALS AND METHODS

Chemicals. CA (CA; ≥98%) was purchased from ChemFaces (Wuhan, China). Ham's F12 complete media, trypsin, fetal bovine serum, penicillin, and streptomycin were supplied by Gibco (MA, USA). 3-(4,5-Dimethyl-2-thiazolyl)-2,5-diphenyl-2H-tetrazolium bromide (MTT; ≥98%) was purchased from Merck KGaA (Darmstadt, Germany). Dimethyl sulfoxide (DMSO; ≥99.9%) was purchased from RCI Labscan Limited, Bangkok, Thailand. Rabbit anti-Bax polyclonal antibody and rabbit anti-Bcl-2 polyclonal antibody were purchased from Proteintech (IL, USA). Rabbit anti-cytochrome *c* monoclonal antibody was obtained from Cell Signaling, MA, USA.

Cell Lines and Cell Culture. KKU-213A (JCRB1557) and KKU-213B (JCRB1556) CCA cell lines, obtained from the Japanese Collection of Research Bioresources (JCRB) Cell Bank and Cholangiocarcinoma Research Institute (CARI), Khon Kaen University, Khon Kaen, Thailand, were cultured in Ham's F12 complete medium (Gibco, MD, USA), which was supplemented with 10% fetal bovine serum, 100 U/mL penicillin, and 100 μg/mL streptomycin. The cells were maintained at 37 °C in a humidified atmosphere containing 5% CO_2. The culture medium was changed every other day. Subculturing was performed when the cells reached an approximate confluence of 80%.

CA Preparation. To prepare a 50 mM stock solution of CA in 100% DMSO, CA was dissolved in DMSO, aliquoted, and stored at −20 °C until use. The stock solution was diluted in complete medium to reach a final concentration of 125 μM CA containing 0.25% DMSO. Different concentrations of CA were prepared by diluting the solution with 0.25% DMSO in complete medium.

Cytotoxicity Assay. CCA cell lines (3×10^3 cells/well in 100 μL) were seeded in 96-well culture plates. Following a culture period of 16 h, cells were treated with various concentrations of CA (5, 10, 15, 20, 25, and 30 μM) in

https://doi.org/10.1021/acsomega.3c07556
ACS Omega 2024, 9, 1278−1286

complete medium containing 0.25% DMSO in triplicate for 24 and 48 h. Control-untreated cells were cultured in complete medium containing 0.25% DMSO. Subsequently, cell morphology was observed under an inverted microscope (Zeiss Axiovert 40, Germany). After 24- and 48 h incubation, the culture medium was removed, and 100 μL of 0.5 mg/mL MTT reagent was added to each well. The plate was incubated in the dark at room temperature for 2 h. After removing the MTT reagent, 100 μL of DMSO was introduced into each well. The plate was incubated for an additional 10 min, and the absorbance was measured at 540 nm using an ELISA microplate reader (Sunrise Tecan, Zurich, Switzerland).

Apoptotic Cell Analysis. CCA cells (8×10^4 cells/well in 2 mL) were seeded into six-well culture plates in triplicate. After culturing for 16 h, cells were treated with various concentrations of CA (15, 20, and 25 μM) in complete medium containing 0.25% DMSO and incubated for 24 h. Control-untreated cells were cultured in complete medium containing 0.25% DMSO. Cellular suspensions were collected and subjected to centrifugation at 2000 rpm for 5 min. Cell pellet was resuspended in 100 μL of binding buffer, pH 7.5. Annexin V-FITC and PI were added as per the manufacturer's instructions (Annexin-V-FLOUS Staining Kit, BD Biosciences, NJ, USA). Cell suspensions were incubated in the dark at room temperature for 15 min. The stained cells were analyzed using flow cytometry with a FACSCanto II instrument (BD Biosciences, NJ, USA) and FlowJo Software version 10 (BD Biosciences, NJ, USA).

Mitochondrial Membrane Potential ($\Delta\Psi$m) Measurement. CCA cells (3×10^4 cells/well in 200 μL) were seeded into 24-well culture plates in triplicate. After culturing for 16 h, cells were treated with different concentrations of CA (15, 20, and 25 μM) in complete medium containing 0.25% DMSO for 24 h. Control-untreated cells were cultured in complete medium containing 0.25% DMSO. Subsequently, cells were stained with JC-1 dye, a component of the JC-1 mitochondrial potential assay kit (Cayman Chemical, MI, USA). Changes in $\Delta\Psi$m were assessed under a confocal laser scanning microscope (Zeiss LSM 980 with Airyscan 2, Jena, Germany) at an excitation/emission wavelength of 485/535 nm. Their red/green fluorescence intensities were quantified by ImageJ software.

Caspase-3 Activity Detection. To detect caspase-3 activity, a colorimetric assay was performed (caspase-3 assay kit; Abcam, Cambridge, UK) following the manufacturer's instructions. Briefly, CCA cells (approximately 3×10^6 cells) were seeded into a 10-cm culture dish and incubated for 16 h. Cells were exposed to 20 μM of CA for 6, 12, and 24 h. The 0-h time point was utilized as a control. Cells were trypsinized and resuspended in 50 μL of chilled cell lysis buffer and incubated on ice for 10 min before centrifuging at 10,000 *g* for 1 min. The supernatant (cytosolic extract) was collected. Protein concentration was measured using the Pierce bicinchoninic acid (BCA) assay kit (Thermo Scientific, MA, USA) and adjusted to 100 μg protein per 50 μL of cell lysis buffer. The supernatant was then added to a mixture of 50 μL of 2× Reaction buffer containing 10 mM dithiothreitol (DTT).DEVD (aspartic acid, glutamic acid, valine, aspartic acid)-*p*-nitroaniline (5 μL, 4 mM) was introduced to the mixture, which was incubated at 37 °C for 1 h. Absorbance at 405 nm was measured using an ELISA microplate reader (Sunrise Tecan, Zurich, Switzerland).

Western Blot Analysis. KKU-213A CCA cells (2×10^7 cells) and KKU-213B CCA cells (3×10^7 cells) were seeded in 10-cm culture dishes, cultured for 16 h, and exposed to 20 μM CA for 6, 12, and 24 h. The 0-h time point was used as a control. Cells were washed with PBS and lysed with radioimmunoprecipitation assay buffer, which contained a protease K inhibitor cocktail [0.5 M NaF, 0.2 M $NaVO_4$, 1 M Tris-HCl at pH 7.5, 0.5 M EDTA, 2.5 M NaCl, 10% sodium dodecyl sulfate (SDS), and deionized water]. Protein concentration was measured using the Pierce BCA assay kit (Thermo Scientific, MA, USA). Subsequently, 20 μg of protein was separated by 10% SDS-polyacrylamide gel electrophoresis, transferred to a polyvinylidene fluoride membrane (Bio-Rad, CA, USA), and blocked with Tris-buffered saline with 0.1% Tween 20 (TTBS) containing 5% skim milk for Bax and Bcl-2 or 5% bovine serum albumin (BSA) for cytochrome *c* for 1 h at room temperature to prevent nonspecific binding. The membrane was incubated with anti-Bax in 1% skim milk (1:2000) anti-Bcl-2 in 5% skim milk (1:2000) or anti-cytochrome c in 5% BSA (1:1000). After overnight incubation at 4 °C, the blot was probed with the corresponding horseradish peroxidase-conjugated secondary antibodies (anti-rabbit at 1:4000 dilution in TTBS for Bax, antirabbit at 1:4000 dilution in 5% skim milk for Bcl-2, and antirabbit at 1:2000 dilution in TBS for cytochrome *c*) for 1 h and rinsed with TTBS. The signals were detected using enhanced chemiluminescence reagent (GE Healthcare UK Ltd., UK) using a Biomolecular imager/ImageQuant 800 (Cytiva, Amersham, UK).

MD Simulations. System preparation: the crystal structure of Bcl-2 (PDB ID: 6GL8)[37] was downloaded from the Protein Data Bank. The structure of CA (ID 6918774) was obtained from the PubChem database. The protonation states of CA were determined at pH 7.4 using MarvinSketch, while those of all ionizable amino acids of Bcl-2 were characterized at the same pH using the PROPKA 3.0 web server. The CA/Bcl-2 complex was prepared using the CDOCKER module implemented in Accelrys Discovery Studio 2.5[Accelrys Inc.]. The partial atomic charges and parameters of CA were computed using the semiempirical AM1-BCC charge model. The force fields AMBER GAFF2 and ff14SB were applied for the ligand and protein, respectively. The LeaP module was employed to add missing hydrogen atoms and TIP3P water molecules[38] to the system. After that, the whole system was energetically minimized using 1500 steps of the steepest descent and 1500 steps of conjugated gradient methods.

MD simulations were run under periodic boundary conditions with the isobaric-isothermal (*NPT*) ensemble using pmemd.cuda in AMBER20. The particle mesh Ewald summation method was employed to treat long-range electrostatic interactions, while a 10 Å distance cutoff was applied for the short-range nonbonded interactions. The SHAKE algorithm was utilized to constrain covalent bonds involving hydrogen atoms. The system was heated from 10 to 298 K over 100 ps. Then, an MD simulation with a time step of 2 fs was performed at 298 K and 1 atm until 100 ns. The CPPTRAJ module[39] of AMBER20 was used for structural analysis, including the RMSD, #contacts, SASA, and hydrogen bond (H-bond) formation. The $\Delta G_{\text{bind}}^{\text{residue}}$ value based on the MM/GBSA method was calculated on the last 20 ns of the simulation.

Statistical Analysis. Three independent triplicates were performed for each experiment. Data were presented as mean

https://doi.org/10.1021/acsomega.3c07556
ACS Omega 2024, 9, 1278−1286

± standard deviation. Statistical significance between groups was evaluated using Student's t test. A p-value of <0.05 was considered statistically significant. All statistical analyses were conducted using GraphPad Prism 8.0.2 (GraphPad Software Inc., USA).

AUTHOR INFORMATION

Corresponding Author

Chadamas Sakonsinsiri − *Department of Biochemistry, Faculty of Medicine, Khon Kaen University, Khon Kaen 40002, Thailand; Cholangiocarcinoma Research Institute, Khon Kaen University, Khon Kaen 40002, Thailand;* orcid.org/0000-0003-0145-8753; Phone: +66-43-363265; Email: schadamas@kku.ac.th

Authors

Onanong Jedram − *Department of Biochemistry, Faculty of Medicine, Khon Kaen University, Khon Kaen 40002, Thailand; Cholangiocarcinoma Research Institute, Khon Kaen University, Khon Kaen 40002, Thailand*

Pornpattra Maphanao − *Department of Biochemistry, Faculty of Medicine, Khon Kaen University, Khon Kaen 40002, Thailand; Cholangiocarcinoma Research Institute, Khon Kaen University, Khon Kaen 40002, Thailand*

Kun Karnchanapandh − *Structural and Computational Biology Research Unit, Department of Biochemistry, Faculty of Science, Chulalongkorn University, Bangkok 10330, Thailand*

Panupong Mahalapbutr − *Department of Biochemistry, Faculty of Medicine, Khon Kaen University, Khon Kaen 40002, Thailand;* orcid.org/0000-0003-4389-334X

Raynoo Thanan − *Department of Biochemistry, Faculty of Medicine, Khon Kaen University, Khon Kaen 40002, Thailand; Cholangiocarcinoma Research Institute, Khon Kaen University, Khon Kaen 40002, Thailand*

Complete contact information is available at: https://pubs.acs.org/10.1021/acsomega.3c07556

Notes

The authors declare no competing financial interest.

ACKNOWLEDGMENTS

This research was supported by the Fundamental Fund of Khon Kaen University from the National Science, Research and Innovation Fund (NSRF) and the Research Fund for Supporting Lecturer to Admit High Potential Student to Study and Research on His Expert Program Year 2020, Graduate School, Khon Kaen University (631JH108). The authors would like to thank Dr. Thanyada Rungrotmongkol from the Structural and Computational Biology Research Unit, Department of Biochemistry, Faculty of Science, Chulalongkorn University for providing computing resources.

ABBREVIATIONS

CCA, cholangiocarcinoma; CA, corosolic acid; GC, gemcitabine plus cisplatin; MD, molecular dynamics; RMSD, root-mean-square displacement; SASA, solvent-accessible surface area; MM/GBSA, molecular mechanics/generalized Born surface area; MTT, 3-(4,5-dimethyl-2-thiazolyl)-2,5-diphenyl-2H-tetrazolium bromide; Annexin V-FITC, FITC-labeled Annexin; PI, propidium iodide; JC-1, 5,5′,6,6′-tetrachloro-1,1′,3,3′-tetraethylbenzimidazolylcarbocyanine iodide; ROS, reactive oxygen species; DMSO, dimethyl sulfoxide; SDS, sodium dodecyl sulfate

REFERENCES

(1) Sripa, B.; Pairojkul, C. Cholangiocarcinoma: lessons from Thailand. *Curr. Opin. Gastroenterol.* **2008**, *24* (3), 349−356.

(2) Kamsa-ard, S.; Kamsa-ard, S.; Luvira, V.; Suwanrungruang, K.; Vatanasapt, P.; Wiangnon, S. Risk factors for cholangiocarcinoma in Thailand: a systematic review and meta-analysis. *Asian Pac. J. Cancer Prev.* **2018**, *19*, 605−614.

(3) Rizvi, S.; Gores, G. J. Pathogenesis, diagnosis, and management of cholangiocarcinoma. *Gastroenterology* **2013**, *145* (6), 1215−1229.

(4) Valle, J. W.; Furuse, J.; Jitlal, M.; Beare, S.; Mizuno, N.; Wasan, H.; Bridgewater, J.; Okusaka, T. Cisplatin and gemcitabine for advanced biliary tract cancer: a meta-analysis of two randomised trials. *Ann. Oncol.* **2014**, *25* (2), 391−398.

(5) Ahn, D. H.; Reardon, J.; Ahn, C. W; Bupathi, M.; Mikihail, S.; Wu, C.S.; Bekaii-Saab, T. Biweekly cisplatin and gemcitabine in patients with advanced biliary tract cancer. *Inter. J. Cancer.* **2017**, *142*, 1671−1675.

(6) Alizadeh, E.; Castle, J.; Quirk, A.; Taylor, C. D. L.; Xu, W.; Prasad, A. Cellular morphological features are predictive markers of cancer cell state. *Comput. Biol. Med.* **2020**, *126*, 104044.

(7) Fink, S. L.; Cookson, B. T. Apoptosis, pyroptosis, and necrosis: mechanistic description of dead and dying eukaryotic cells. *Infect. Immun.* **2005**, *73* (4), 1907−1916.

(8) Bailey, R. W.; Nguyen, T.; Robertson, L.; Gibbons, E.; Nelson, J.; Christensen, R. E.; Bell, J. P.; Judd, A. M.; Bell, J. D. Sequence of physical changes to the cell membrane during glucocorticoid-induced apoptosis in S49 lymphoma cells. *Biophys. J.* **2009**, *96* (7), 2709−2718.

(9) Teijido, O.; Dejean, L. Upregulation of Bcl2 inhibits apoptosis-driven BAX insertion but favors BAX relocalization in mitochondria. *FEBS Lett.* **2010**, *584* (15), 3305−3310.

(10) Perlman, H.; Zhang, X.; Chen, M. W.; Walsh, K.; Buttyan, R. An elevated bax/bcl-2 ratio corresponds with the onset of prostate epithelial cell apoptosis. *Cell Death Differ.* **1999**, *6* (1), 48−54.

(11) Raisova, M.; Hossini, A. M.; Eberle, J.; Riebeling, C.; Orfanos, C. E.; Geilen, C. C.; Wieder, T.; Sturm, I.; Daniel, P. T. The Bax/Bcl-2 ratio determines the susceptibility of human melanoma cells to CD95/Fas-mediated apoptosis. *J. Invest. Dermatol.* **2001**, *117* (2), 333−340.

(12) Bossy-Wetzel, E.; Green, D. R. Caspases induce cytochrome c release from mitochondria by activating cytosolic factors. *J. Biol. Chem.* **1999**, *274* (25), 17484−17490.

(13) Ulbricht, C.; Dam, C.; Milkin, T.; Seamon, E.; Weissner, W.; Woods, J. Banaba (*Lagerstroemia speciosa* L.): An evidence-based systematic review by the Natural Standard Research Collaboration. *J. Herb. Pharmacother.* **2007**, *7*, 99−113.

(14) Kim, J. H.; Kim, Y. H.; Song, G. Y.; Kim, D. E.; Jeong, Y. J.; Liu, K. H.; Chung, Y. H.; Oh, S. Ursolic acid and its natural derivative corosolic acid suppress the proliferation of APC-mutated colon cancer cells through promotion of β-catenin degradation. *Food Chem. Toxicol.* **2014**, *67*, 87−95.

(15) Ku, C. Y.; Wang, Y. R.; Lin, H. Y.; Lu, S. C.; Lin, J. Y. Corosolic acid inhibits hepatocellular carcinoma cell igration by targeting the VEGFR2/Src/FAK pathway. *PLoS One* **2015**, *10*, No. e0126725.

(16) Xu, Y.; Zhao, Y.; Xu, Y.; Guan, Y.; Zhang, X.; Chen, Y.; Wu, Q.; Zhu, G.; Chen, Y.; Sun, F.; et al. Blocking inhibition to YAP by ActinomycinD enhances anti-tumor efficacy of Corosolic acid in treating liver cancer. *Cell. Signal.* **2017**, *29*, 209−217.

(17) Yoo, K. H.; Park, J. H.; Lee, D. Y.; Hwang-Bo, J.; Baek, N. I.; Chung, I. Corosolic acid exhibits nti-angiogenic and anti-lymphangiogenic effects on *in vitro* endothelial ells and on an *in vivo* CT-26 colon carcinoma animal model. *Phytother. Res.* **2015**, *29*, 714−723.

(18) Zhao, J.; Zhou, H.; An, Y.; Shen, K.; Yu, L. Biological effects of corosolic acid as an anti-inflammatory, anti-metabolic syndrome and anti-neoplasic natural compound (Review). *Oncol. Lett.* **2020**, *21*, 84.

https://doi.org/10.1021/acsomega.3c07556
ACS Omega 2024, 9, 1278−1286

(19) Cheng, Q. L.; Li, H. L.; Li, Y. C.; Liu, Z. W.; Guo, X. H.; Cheng, Y. J. CRA(Crosolic Acid) isolated from *Actinidia valvata* Dunn.Radix induces apoptosis of human gastric cancer cell line BGC823 *in vitro* via down-regulation of the NF-κB pathway. *Food Chem. Toxicol.* **2017**, *105*, 475−485.
(20) Sung, B.; Kang, Y.; Kim, D.; Hwang, S. Y.; Lee, Y.; Kim, M.; Yoon, J. H.; Kim, C.; Chung, H. Y.; Kim, N. D. Corosolic acid induces apoptotic cell death in HCT116 human colon cancer cells through a caspase-dependent pathway. *Int. J. Mol. Med.* **2014**, *33*, 943−949.
(21) Nho, K. J.; Chun, J. M.; Kim, H. K. Corosolic acid induces apoptotic cell death in human lung adenocarcinoma A549 cells in vitro. *Food Chem. Toxicol.* **2013**, *56*, 8−17.
(22) Cai, X.; Zhang, H.; Tong, D.; Tan, Z.; Han, D.; Ji, F.; Hu, W. Corosolic acid triggers mitochondria and caspase-dependent apoptotic cell death in osteosarcoma MG-63 cells. *Phytother Res.* **2011**, *25* (9), 1354−1361.
(23) Fujiwara, Y.; Komohara, Y.; Ikeda, T.; Takeya, M. Corosolic acid inhibits glioblastoma cell proliferation by suppressing the activation of signal transducer and activator of transcription-3 and nuclear factor-kappa B in tumor cells and tumor-associated macrophages. *Cancer Sci.* **2011**, *102* (1), 206−211.
(24) Zhang, C.; Niu, Y.; Wang, Z.; Xu, X.; Li, Y.; Ma, L.; Wang, J.; Yu, Y. Corosolic acid inhibits cancer progression by decreasing the level of CDK19-mediated O-GlcNAcylation in liver cancer cells. *Cell Death Dis.* **2021**, *12* (10), 889.
(25) Jasim, S. A.; Khalaf, O. Z.; Alshahrani, S. H.; Hachem, K.; Ziyadullaev, S.; Jalil, A. T.; Wang, C.; Zabibah, R. S.; Jardan, Y. A. B.; Qasim, Q. A.; et al. An *in vitro* investigation of the apoptosis-inducing activity of corosolic acid in breast cancer cells. *Iran. J. Basic Med. Sci.* **2023**, *26* (4), 453−460.
(26) Ma, B.; Zhang, H.; Wang, Y.; Zhao, A.; Zhu, Z.; Bao, X.; Sun, Y.; Li, L.; Zhang, Q. Corosolic acid, a natural triterpenoid, induces ER stress-dependent apoptosis in human castration resistant prostate cancer cells via activation of IRE-1/JNK, PERK/CHOP and TRIB3. *J. Exp. Clin. Cancer Res.* **2018**, *37* (1), 210.
(27) Kongpetch, S.; Kukongviriyapan, V.; Prawan, A.; Senggunprai, L.; Kukongviriyapan, U.; Buranrat, B. Crucial role of heme oxygenase-1 on the sensitivity of cholangiocarcinoma cells to chemotherapeutic agents. *PLoS One* **2012**, *7*, No. e34994.
(28) Matsumoto, H.; Wada, T.; Fukunaga, K.; Yoshihiro, S.; Matsuyama, H.; Naito, K. Bax to Bcl-2 ratio and Ki-67 index are useful predictors of neoadjuvant chemoradiation therapy in bladder cancer. *Jpn. J. Clin. Oncol.* **2004**, *34*, 124−130.
(29) Singh, L.; Pushker, N.; Saini, N.; Sen, S.; Sharma, A.; Bakhshi, S.; Chawla, B.; Kashyap, S. Expression of pro-apoptotic Bax and anti-apoptotic Bcl-2 proteins in human retinoblastoma. *Clin. Exp. Ophthalmol.* **2015**, *43* (3), 259−267.
(30) Tusskorn, O.; Senggunprai, L.; Prawan, A.; Kukongviriyapan, U.; Kukongviriyapan, V. Phenethyl isothiocyanate induces calcium mobilization and mitochondrial cell death pathway in cholangiocarcinoma KKU-M214 cells. *BMC Cancer* **2013**, *13*, 571.
(31) Meijerink, J.; Mensink, E.; Wang, K.; Sedlak, T.; Slöetjes, A. W.; de Witte, T.; Waksman, G.; Korsmeyer, S. Hematopoietic malignancies demonstrate loss-of-function mutations of BAX. *Blood* **1998**, *91*, 2991−2997.
(32) Wang, G.; Nikolovska-Coleska, Z.; Yang, C. Y.; Wang, R.; Tang, G.; Guo, J.; Shangary, S.; Qiu, S.; Gao, W.; Yang, D.; et al. Structure-based design of potent small-molecule inhibitors of anti-apoptotic Bcl-2 proteins. *J. Med. Chem.* **2006**, *49* (21), 6139−6142.
(33) Ji, T.; Margulis, B. A.; Wang, Z.; Song, T.; Guo, Y.; Pan, H.; Zhang, Z. Structure-based design and structure-activity relationship analysis of small molecules inhibiting Bcl-2 family members. *Pharm. Chem. J.* **2022**, *56* (3), 329−338.
(34) Iyer, D.; Vartak, S. V.; Mishra, A.; Goldsmith, G.; Kumar, S.; Srivastava, M.; Hegde, M.; Gopalakrishnan, V.; Glenn, M.; Velusamy, M.; et al. Identification of a novel BCL2-specific inhibitor that binds predominantly to the BH1 domain. *FEBS J.* **2016**, *283* (18), 3408−3437.
(35) Tang, G.; Yang, C. Y.; Nikolovska-Coleska, Z.; Guo, J.; Qiu, S.; Wang, R.; Gao, W.; Wang, G.; Stuckey, J.; Krajewski, K.; et al. Pyrogallol-based molecules as potent inhibitors of the antiapoptotic Bcl-2 proteins. *J. Med. Chem.* **2007**, *50* (8), 1723−1726.
(36) Wei, H.; Wang, H.; Wang, G.; Qu, L.; Jiang, L.; Dai, S.; Chen, X.; Zhang, Y.; Chen, Z.; Li, Y.; et al. Structures of p53/BCL-2 complex suggest a mechanism for p53 to antagonize BCL-2 activity. *Nat. Commun.* **2023**, *14* (1), 4300.
(37) Casara, P.; Davidson, J.; Claperon, A.; Le Toumelin-Braizat, G.; Vogler, M.; Bruno, A.; Chanrion, M.; Lysiak-Auvity, G.; Le Diguarher, T.; Starck, J. B.; et al. S55746 is a novel orally active BCL-2 selective and potent inhibitor that impairs hematological tumor growth. *Oncotarget* **2018**, *9* (28), 20075−20088.
(38) Mark, P.; Nilsson, L. Structure and dynamics of the TIP3P, SPC, and SPC/E water models at 298 K. *J. Phys. Chem. A* **2001**, *105* (43), 9954−9960.
(39) Roe, D. R.; Cheatham, T. E. PTRAJ and CPPTRAJ: Software for processing and analysis of molecular dynamics trajectory data. *J. Chem. Theory Comput.* **2013**, *9* (7), 3084−3095.

https://doi.org/10.1021/acsomega.3c07556
ACS Omega 2024, 9, 1278−1286